

Measurements of Unsteady Pressure Distributions and Dynamic Deformations on an SST Elastic Arrow-Wing Model *

Masato TAMAYAMA *¹, Kenichi SAITOH *², Hiroshi MATSUSHITA *³
Masataka HASHIDATE *⁴, and Jiro NAKAMICHI *¹

ABSTRACT

Unsteady pressure distributions were measured in a series of experiments in the transonic regime for a double-swept-back semi-span SST arrow wing model. The wing is an elastic model, the first natural frequency is 9.79 Hz. Forty-six unsteady pressure transducers and 45 pressure orifices were embedded at two semi-span stations to measure unsteady and steady pressure distributions respectively. The influence of temperature drifts in the wind tunnel could be effectively removed from the pressure transducer signal by timely taking of zero-balance. As a result, the gain of amplifiers was able to be raised, and then high S/N ratio achieved. Dynamic deformation data of the wing model were also measured, using optical targets and CCD cameras. The flow field around the model was excited by a trailing edge flap which was oscillated around a mean deflection angle in the frequency range up to 30 Hz. The model vibration mode changed at the flap frequency near the model 1st resonance. The unsteady pressure distributions were affected by this change of vibration mode. Unsteady lift and moment coefficients were derived from unsteady pressure distributions. Of particular role is the fact that while the unsteady aerodynamic coefficients were affected strongly by the flap motion at the inboard wing section, they were influenced by the wing vibration at the outboard wing section.

Keywords: Unsteady Aerodynamics, Aeroelasticity, Transonic Flow, SST

概 要

2段に後退した半載のSSTアロー翼を用いて、遷音速領域で非定常圧力分布を計測した。翼は1次の固有振動数が9.79Hzの弾性模型である。46点の非定常圧力変換器を埋め込んだ圧力孔と、他に45点の圧力孔を2列のセミスパン位置に設け、非定常及び定常圧力分布を各々計測した。定常及び非定常圧力を別々に計測し、適時にアンプのゼロバランスをとることにより、圧力変換器に生じる温度ドリフトの影響を取り除いた。この結果、アンプゲインの値を高めることが可能となり、S/N比の向上につながった。また翼模型の動的変位データを、光ファイバとCCDカメラを用いて計測した。翼後縁に設けたフラップの運動により、翼周りの流れに非定常性を励起した。フラップは平均舵角周りに最高30Hzの周波数で加振した。実験結果より、模型の振動モードは1次の共振振動数に近いフラップ振動数で変化し、この変化が非定常圧力分布にも現れることが確認できた。揚力及びモーメントの非定常成分は、非定常圧力分布を積分して求めた。また、非定常空力係数に関しては、翼の内舷ではフラップの振動が強く影響し、外舷では翼の振動自体が強く影響することがわかった。

* 平成11年2月12日 受付 (received 12, February 1999)

* 1 構造研究部 (Structures Division)

* 2 次世代航空機プロジェクト推進センター (Advanced Technology Aircraft Project Center)

* 3 特別研究官 (Director of Special Research)

* 4 新型航空機研究グループ

1 . INTRODUCTION

The development of the next generation Super Sonic Transport (SST) is attracting a great attention all over the world, especially in the U.S.A. NASA has promoted High Speed Research (HSR) Program in cooperation with private companies since 1990¹⁾. The next generation SST may be developed as an international cooperative work. In view of this prospect, various researches and feasibility studies on the next generation SST have been also conducted in Japan²⁾. And a national project on SST has been promoted. It includes flight experiments with scaled SST models, which are planned in 2001. One of the most important objects in the project is to establish Japan's own technologies, for instance, design techniques using Computational Fluid Dynamics (CFD) and material technologies.

In the development of CFD codes, it is necessary to verify the codes with experimental data. Many researches on the unsteady aerodynamics have been performed in various forms at transonic speed. Unsteady aerodynamic forces have been often measured on rigid 2D and 3D wings in pitching motions as well as oscillating partial control surfaces³⁻⁵⁾. In most of these researches, unsteady pressures were measured with a tube type system, which is cheaper in cost and, on the contrary, labored in acquiring accurate pressure values. In addition, since a rigid body was assumed, elastic deformations of the model were scarcely taken into account. In order to validate CFD codes for aeroelasticity, unsteady deformation data on elastic models are necessary as well as unsteady aerodynamic data. But few validation data, e.g. the NASA's test data on a Flexible Semi-span Model (FSM)⁶⁾, are available in transonic speed, where an aircraft becomes critical by aeroelasticity problems.

From the above situations, the following necessity arose. That is, in order to evaluate our aeroelasticity CFD code, we should have to manufacture our own elastic model. For the sake of acquiring accurate data, attentions were paid to the following points:

1) In situ pressure transducers were used instead of the tube-pressure transducer system, to avoid the possible problems in the measurement reliability if appropriate corrections are not applied to the data.

2) If the wind tunnel is continuously driven, the temperature drifts in the tunnel during a test influence the pressure transducer signal⁷⁾. In order to eliminate this effect, steady pressure distributions were measured with additional pressure orifices. An improvement in S/N ratio of the unsteady pressure measurements was also led by this procedure, because the amplifier's gain could be increased for the unsteady measurements.

3) The model was installed with optical targets in order to measure the model dynamic deformations⁸⁻¹⁰⁾.

In the CFD analysis at transonic speed, verifications are especially needed on unsteady aerodynamic forces caused by oscillating control surfaces. Our model is installed with a flap in the model rear part, which can be oscillated to generate the unsteady flows.

The details of tests will be described in the following sections. Presenting some results, the relations will be pointed out between unsteady aerodynamics and dynamic deformations.

2 . Wind Tunnel

Tests were conducted in the Transonic Wind Tunnel (TWT)¹¹⁾ at the National Aerospace Laboratory (NAL). No.3 cart was used. There are slots on the upper and lower walls of the cart in order to prevent choking. TWT is a closed circulatory wind tunnel. The range of Mach numbers and total pressures in TWT are from 0.1 to 1.4 and from 50 kPa to 150 kPa, respectively. The test section size is 2 m by 2 m. The model supporting fixture is in the side wall. The angles of attack and the dihedral angles can be changed in ranges of ± 20 and ± 5 degrees, respectively.

3 . Wind Tunnel Model

The model tested in TWT is a double-swept-back semi-span SST arrow wing¹²⁾. The planform of the model is shown in Fig.1. The root length of the wing is 2.10 m and the span from the tunnel side wall to the wing tip is 1.00 m. The mean aerodynamic chord length is 1.27 m. Figure 2 shows the model mounted in TWT. The cross section is NACA0003 airfoil at every span position. The flap at the end of inboard wing can produce unsteady flow fields around the wing.

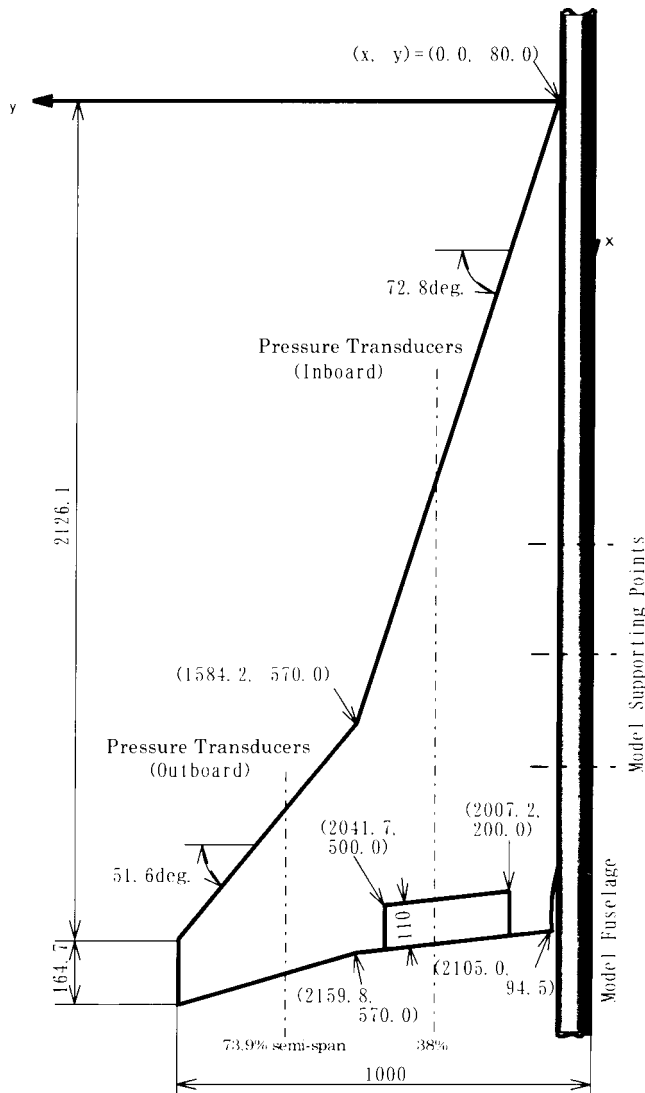


Figure 1. Model Planform



Figure 2. Model in TWT

Table 1. Natural Frequencies and Generalized Mass of Model

| Mode | Natural Frequency [Hz] | | Generalized Mass [kg] |
|------|------------------------|---------------|-----------------------|
| | FEM | VibrationTest | |
| 1 | 11.09 | 9.79 | 5.1982 |
| 2 | 41.65 | | 2.3109 |
| 3 | 44.00 | 40.25 | 3.2874 |
| 4 | 56.26 | 47.91 | 1.9764 |
| 5 | 89.49 | 64.19 | 1.4333 |
| 6 | 119.23 | 90.57 | 0.7928 |
| 7 | 145.44 | 111.04 | 2.0683 |
| 8 | 163.58 | 122.39 | 1.2810 |

Table 1 lists the natural frequencies of the model obtained by FEM analysis together with the results of the vibration test. The generalized masses calculated by FEM analysis are also informed in Tab.1. Figure 3 illustrates the mode contours computed by FEM analysis, which are normalized by the maximum displacement of each mode.

Forty-six pressure transducers are installed at two semi-span positions as indicated in Fig.1. The type of the transducer is Kulite XCS-062. Figure 4 shows the location of the transducers with the identification numbers. The uncertainty of the measured unsteady pressure was about $\pm 0.46\%$ against the actual pressure value. In this calculation, the thermal sensitivity and the repeatability of transducers were considered under the test conditions to be described in the paragraph 4.1. Pressure orifices are located 4mm beside the pressure transducer's orifices except for No. 21 and they are utilized for the steady pressure measurements.

Twenty-one optical targets are installed at five semi-span positions which are shown in Fig.5. The dynamic deformation was measured with these targets. Two accelerometers are installed at each span of 66.8 % and 84.7%.

4 . Experimental Description

4.1 Test Condition

The results presented here was acquired at Mach number, M , 0.851, total pressure, P_o , 80.0 kPa, total temperature, T_o , 310 K and Reynolds number, 1.05×10^7 /m. The angle of attack of the wing, ,

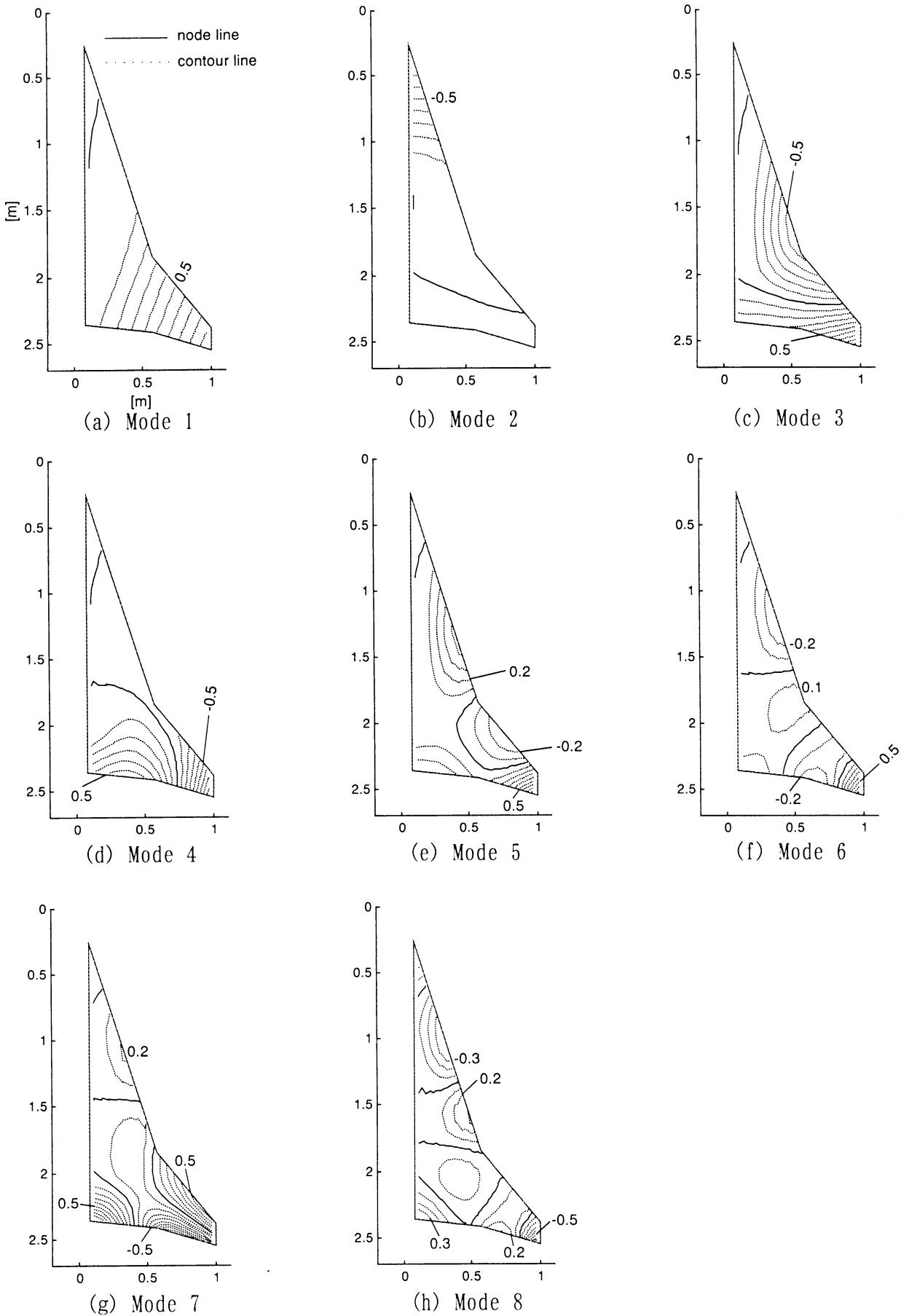
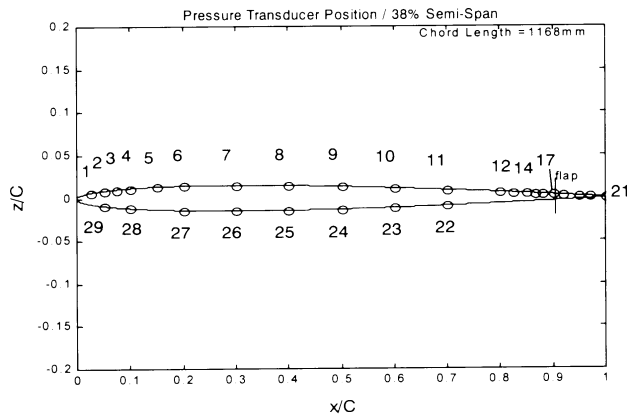
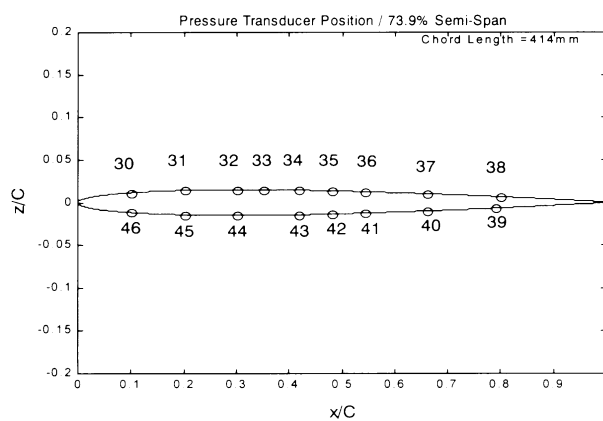


Figure 3. Natural Modes Acquired by FEM Analysis



(a) 38% Semi-Span



(b) 73.9% Semi-Span

Figure 4. Location of Pressure Transducers

was set to 0 degree. The mean value of the flap deflection angle, α , was also set to 0 degree. The amplitude of the flap oscillations was around 2 degrees. The flap was excited in sinusoidal motions. The downward flap deflection was defined as positive. The frequencies of the flap oscillations, f , were 5, 10, 15, 20, 25 and 30 Hz, whose corresponding reduced frequencies, k , were 0.12, 0.24, 0.35, 0.47, 0.59, and 0.71, respectively. k is equal to $2fb/U$, where b is the semi-root-chord length, and where U is the free stream velocity.

4.2 Data Acquisition

Digital data from all of the pressure transducers and accelerometers were acquired simultaneously by HiDAP (High speed Data Acquisition Processing) system equipped in TWT. The sampling frequency was 25.6 kHz. This sampling frequency was chosen in order to observe the propagation of flow perturbations¹³⁾. The total sampling time was 60 seconds with the frequencies changed from 5 to 30 Hz. In this re-

| Location of Accelerometers | | | |
|----------------------------|-------|-----------------|-------|
| 66.8% Semi-Span | | 84.7% Semi-Span | |
| No. | % x/C | No. | % x/C |
| 1 | 30.0 | 2 | 30.0 |
| 3 | 65.0 | 4 | 65.0 |

○ (●) Optical Target
□ Accelerometer

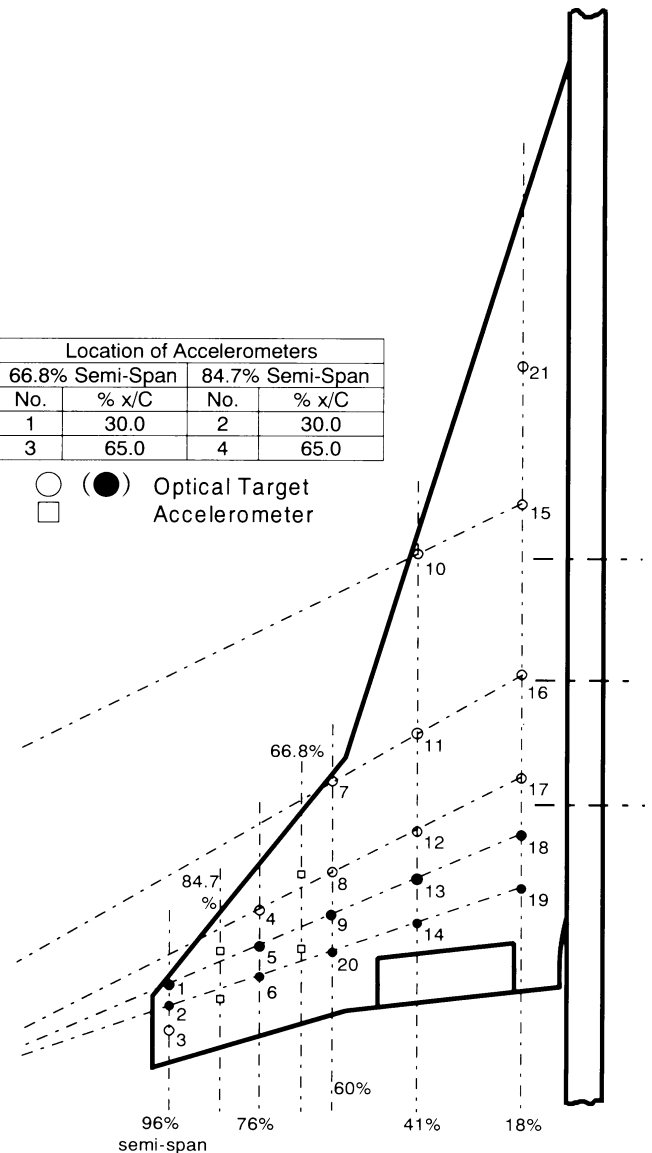


Figure 5. Location of Optical Targets and Accelerometers

port, attentions are paid to the low frequency phenomena caused by the flap motions. The sampling frequency of the data, therefore, was reduced to 256 Hz by the use of a digital filter. Two scanning valves were connected to the pressure orifices provided for the steady pressure measurements.

4.3 Dynamic Deformation Measurement (DDM)

Figure 6 schematically shows the Dynamic Deformation Measurement (DDM) system⁹⁾. All targets consist of optical fibers. The targets at 18%, 41% and 60% semi-span positions were connected to a strong light source behind the tunnel side wall. The targets at 76% and 96% semi-span positions were led to the wing lower surface and supplied with light by search-

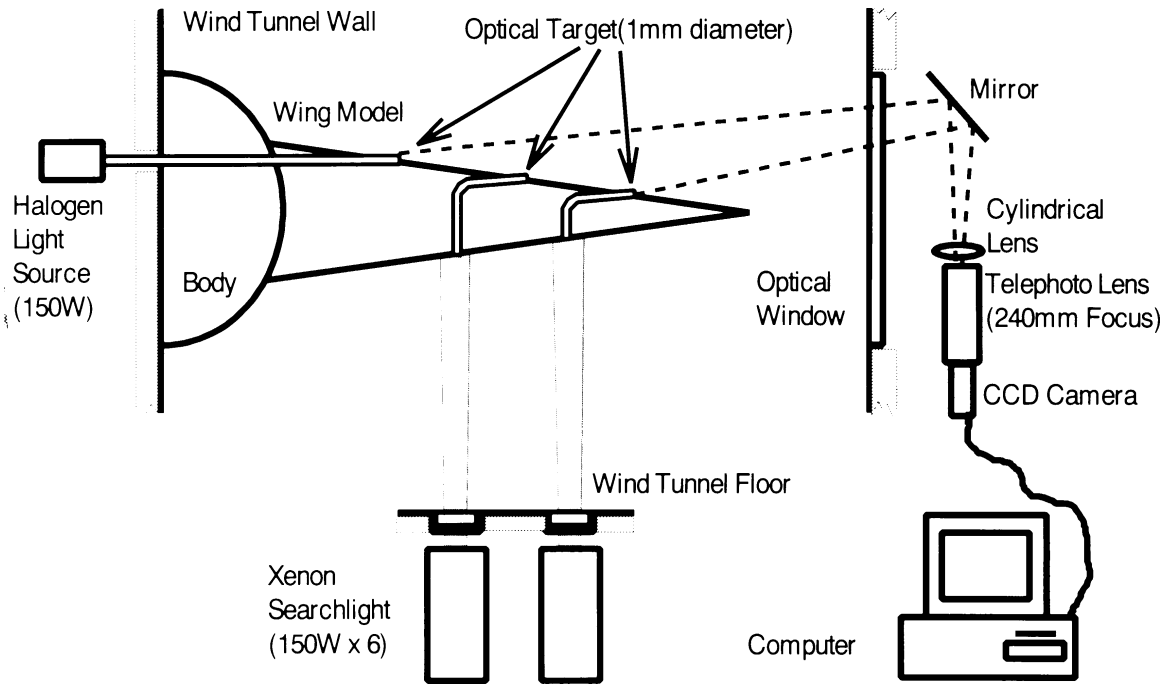


Figure 6. Dynamic Deformation Measurement (DDM) System

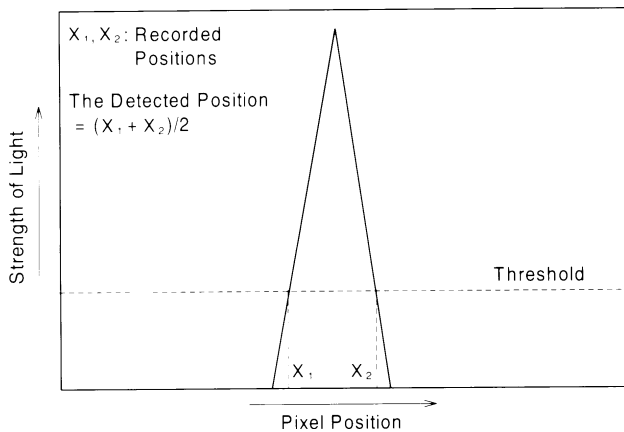


Figure 7. Detection of Optical Targets

lights mounted below the test section floor. Light of targets was traced with CCD cameras. Each camera had 3,648 sensing elements (pixels) arranged in a line. A target image was represented by pixels with a range of light intensity. Figure 7 shows an image of light intensity distributions. Only the pixels crossing a threshold intensity level were recorded. The target position was, then, detected as the center of the recorded pixel positions x_1 and x_2 . The sampling frequency was 333Hz. The resolution of measurements was about 40 to 60 μ m. Each target had its individual resolution. The total sampling time was 60 seconds.

5 . Results and Discussion

5.1 DDM

Figure 8 shows the measured dynamic deformations by DDM. The results from the optical targets indicated by black spots, , in Fig.5 are analyzed. The data are translated into the heaving and the pitching components. These components are defined as follows:

As for the heaving component, h is expressed by

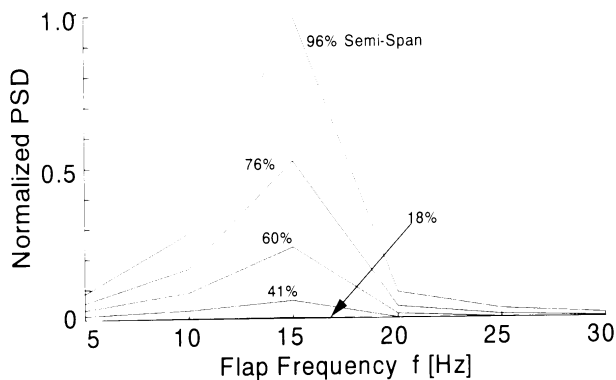
$$h = \frac{z_1 + z_2}{2} \dots\dots\dots (1)$$

and the pitching component, is expressed by

$$= \frac{z_1 - z_2}{2d} \dots\dots\dots (2)$$

where z_1 and z_2 are the deformations of forward and rearward targets at each semi-span position, respectively. d is the chord wise distance between these two targets. Figure 8 presents power spectrum densities (PSD) of transfer functions of h and vs. flap motions. The PSD quantities are normalized by the maximum values in each graph.

The figure shows a peak at $f = 15$ Hz, especially strong at the wing tip part. Figure 9 shows the PSD of accelerometer output in case of no flap motions. The first resonant frequency is about 13.5 Hz. Therefore, the model suffered almost a resonant vibration at $f = 15$ Hz, which was observed in a video monitor, too. h



(a) Heaving Component

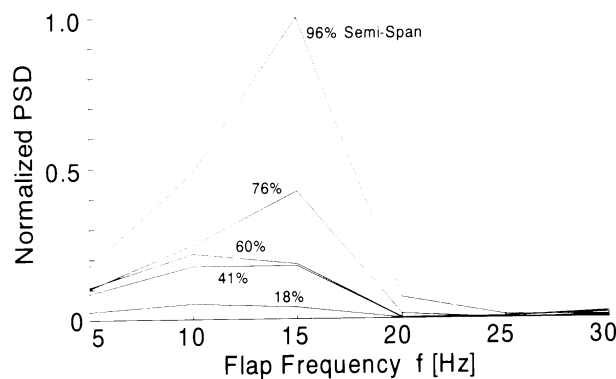


Figure 8. Vibration at Model Rear Part

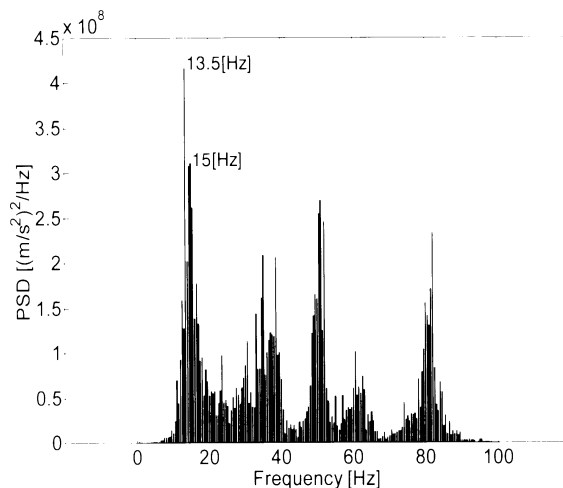
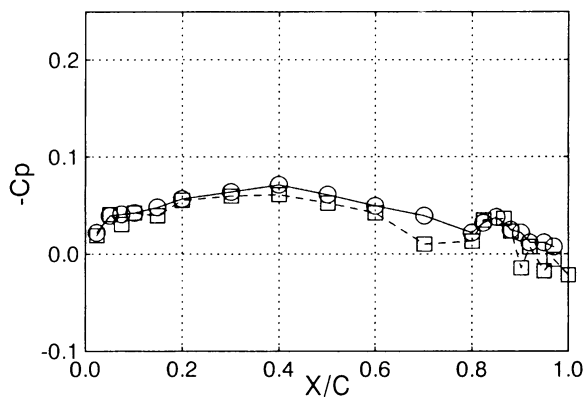


Figure 9. PSD of Accelerometer Signal

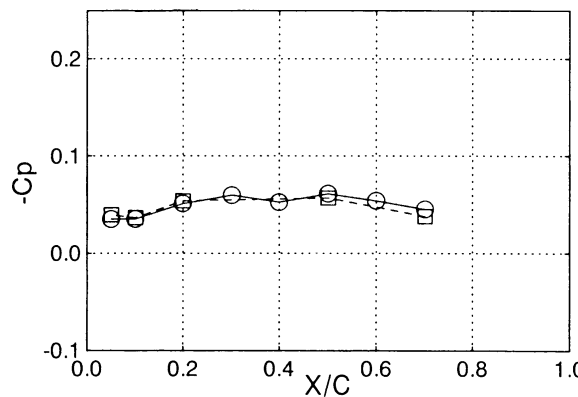
and are stronger at the lower frequencies, especially remarkable in .

5.2 Pressure - Steady Component

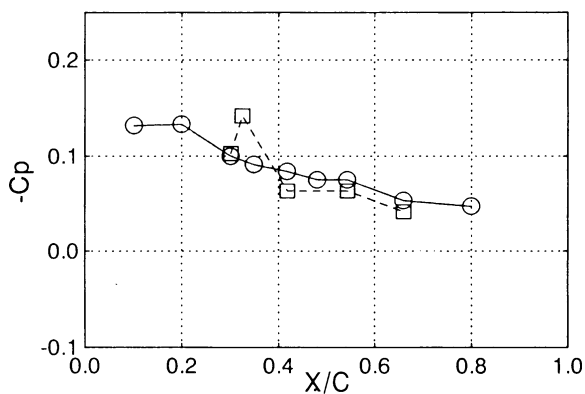
Figure 10 shows the distributions of the mean pressure coefficients, C_p . The symbols, and , represent the data from the pressure transducers⁷⁾ and the scanning valves connected with pressure orifices, respectively. More unevenness is apparent in the



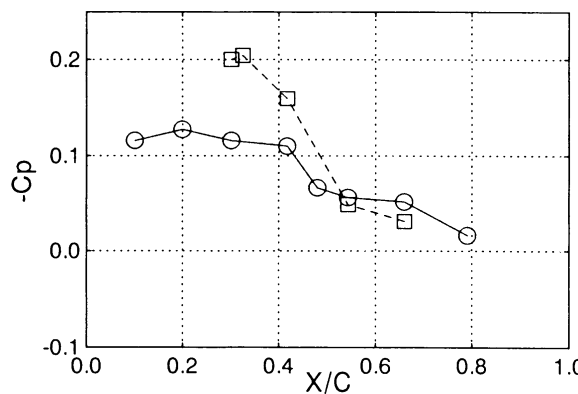
(a) Inboard Upper



(b) Inboard Lower



(c) Outboard Upper



(d) Outboard Lower

Figure 10. Pressure Distributions - Steady Component

(: Measured with Scanning Valves, : Average of Unsteady Pressure Transducer Signal)

former. This unevenness is caused by the temperature drifts in TWT. Since the sensitivity to the temperature depends upon transducers, the unevenness appears in their distributions. There is the difficulty that we can not take zero-balance during the test if we want to derive the mean pressure from unsteady pressure data. In order to remove the influence of temperature drifts in the wind tunnel, we measured the steady pressure distributions not with in situ transducers, but a tube-scanning valve system. The distributions indicated by circles show improvements and are able to provide wider and more detailed distributions than those indicated by squares.

The distributions on both the upper and lower surfaces agree with each other. At the outboard section, the distributions show higher $-C_p$ than those at the inboard section. It is considered that this tendency is caused by the wing surface conditions and the 3D flow effects in the outboard region.

5.3 Pressure - Unsteady Component

Figure 11 shows the unsteady component of pressure fluctuations normalized by the flap oscillations. The flap oscillation is expressed as

$$= | \quad | e^{i2 \quad \dot{f} t} \quad \dots\dots\dots(3)$$

The unsteady component of pressure fluctuation is

$$C_p = | \quad C_{p|} e^{i(2 \quad \dot{f} t \quad)} \quad \dots\dots\dots(4)$$

Therefore, the transfer function becomes as

$$G = |G| e^{i \quad } \\ = \quad C_p \\ = \quad \frac{| \quad C_{p|}}{| \quad |} e^{-i \quad } \quad \dots\dots\dots(5)$$

The $|G|$ distributions on the inboard upper surface peak at $x/C = 0.9$ for every flap frequency, where x and C denote the local chordwise position from the wing leading edge and the local chord length, respectively. $x/C = 0.9$ means the position located immediately in front of the flap hinge line. The peak values do not depend on the flap frequencies. They are considered to be affected by the flap motion itself rather than the global model vibration. Since the wing has a symmetrical cross section and $\alpha = 0$ degree, the $|G|$ distributions show almost the same aspect on both the upper and the lower surfaces.

The $|G|$ distributions show different behaviors as the flap frequencies increase. Minimum values are observed in both the inboard and outboard distribu-

tions at $f = 10$ Hz, e.g. at $x/C=0.7$ of the inboard section. The phase, ϕ , jumps about 180 degrees around the same chordwise points as the minimum locations and it shifts continuously. This might express the influences of model vibration mode. The vibration modes include a strong pitching component in this frequency range, which was stated in the paragraph 5.1.

The minimum values mentioned above are not observed in the distributions at $f = 15$ Hz. $|G|$ decreases as frequencies increase. A half cycle phase jump is not observed in the ϕ distributions. The pitching component of wing vibration attenuates its influences comparing with the heaving component. At each f , $|G|$ is larger in the outboard wing than that in the inboard wing, that is, the outboard wing vibrates more violently.

5.4 Aerodynamic Forces

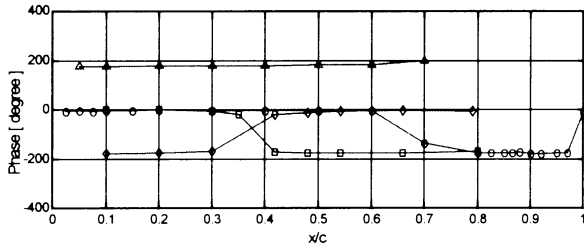
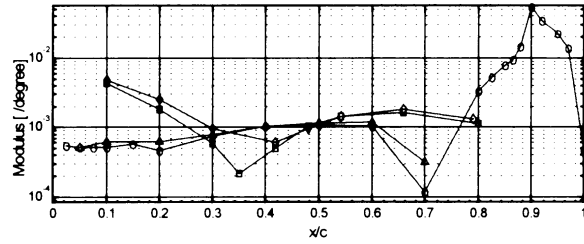
Figure 12 shows the time histories of the unsteady components of lift and moment coefficients, C_l and C_m , at the inboard and the outboard sections. Each coefficient is defined as follows:

$$C_l = \frac{l}{qC} \quad \dots\dots\dots(6)$$

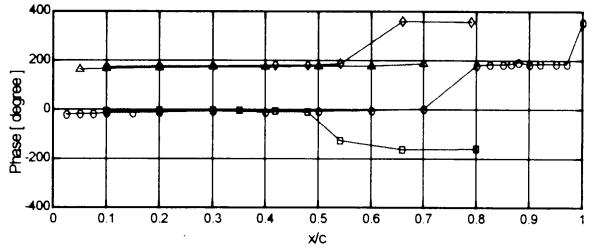
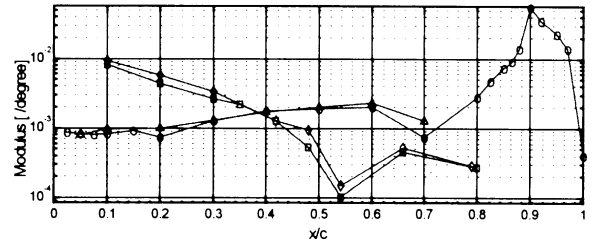
$$C_m = \frac{m}{qC^2} \quad \dots\dots\dots(7)$$

l and m are the local lift and the moment acting on unit span width. q is the free stream dynamic pressure. The local aerodynamic forces were derived from integrating unsteady pressure distributions. At the wing leading edge, the unsteady pressure was assumed as 0 kPa. At the outboard trailing edge, the unsteady pressures were individually extrapolated for each of the upper and the lower surfaces. Then, the average of these values was taken and assumed as the unsteady pressure value at the outboard trailing edge. m was calculated around 25 % chord position. The pitch-up moment was taken as positive.

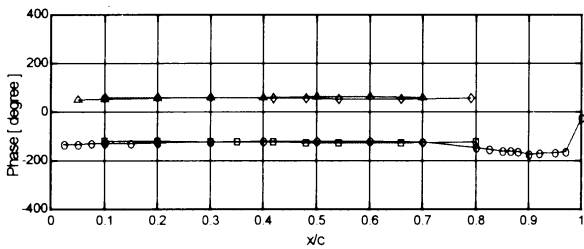
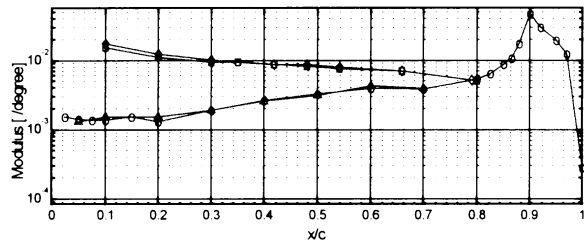
The amplitude of aerodynamic coefficients is greatest at $f = 15$ Hz. A resonance with the wing 1st mode causes a violent vibration, which seems remarkable particularly in the outboard C_l . While C_l and C_m at the inboard sections are affected strongly by the flap motion itself, those at the outboard sections are strongly influenced by the wing vibration mode.



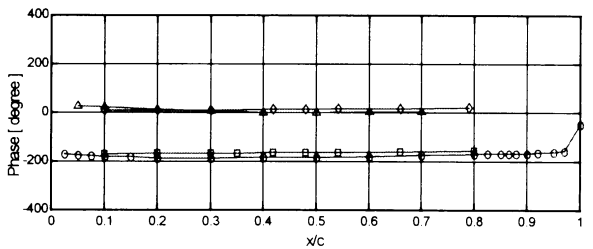
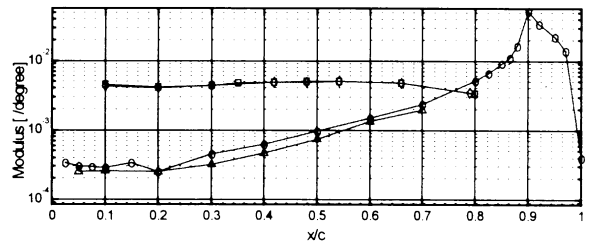
(a) $f = 5$ [Hz]



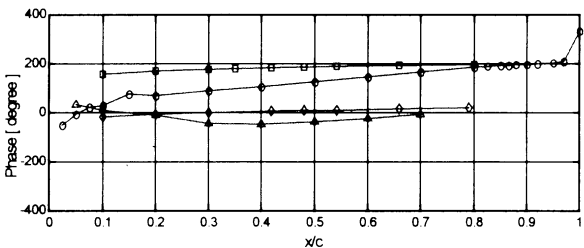
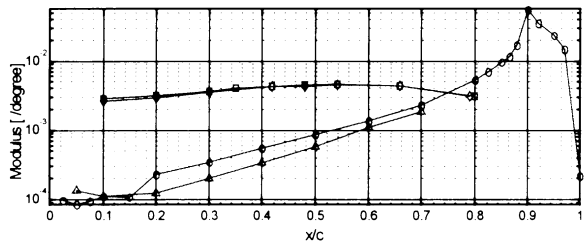
(b) $f = 10$ [Hz]



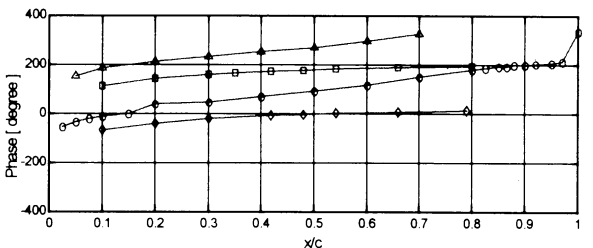
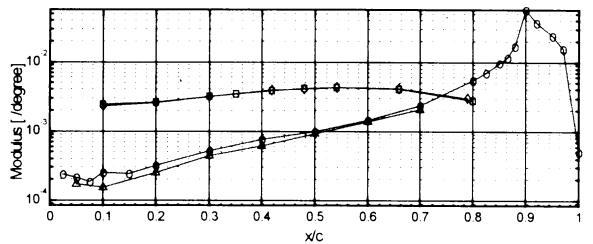
(c) $f = 15$ [Hz]



(d) $f = 20$ [Hz]



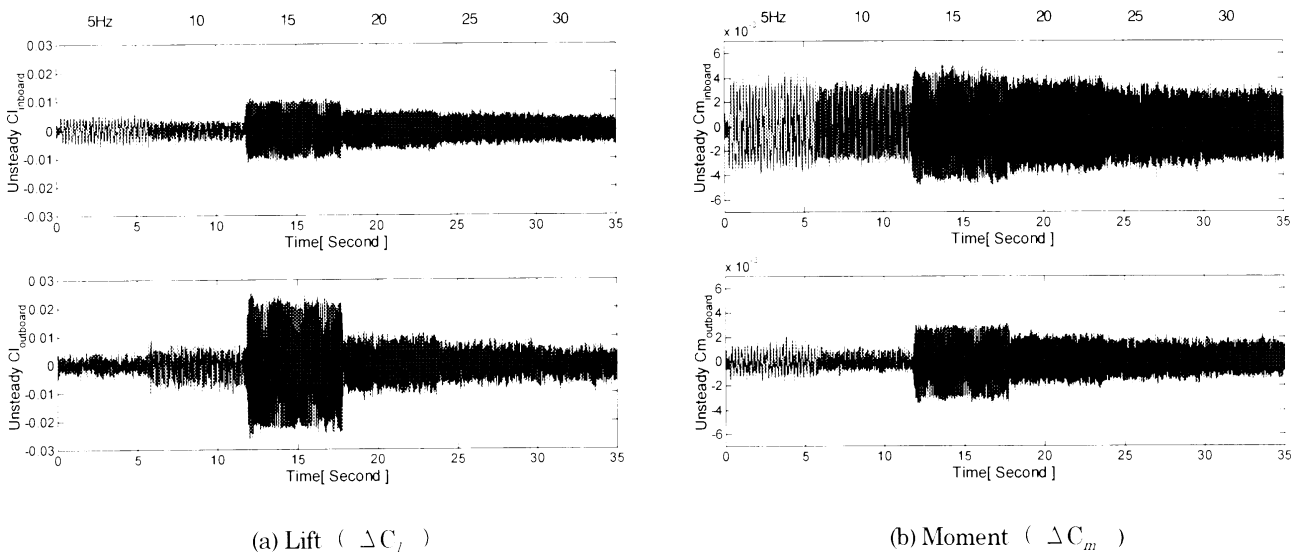
(e) $f = 25$ [Hz]



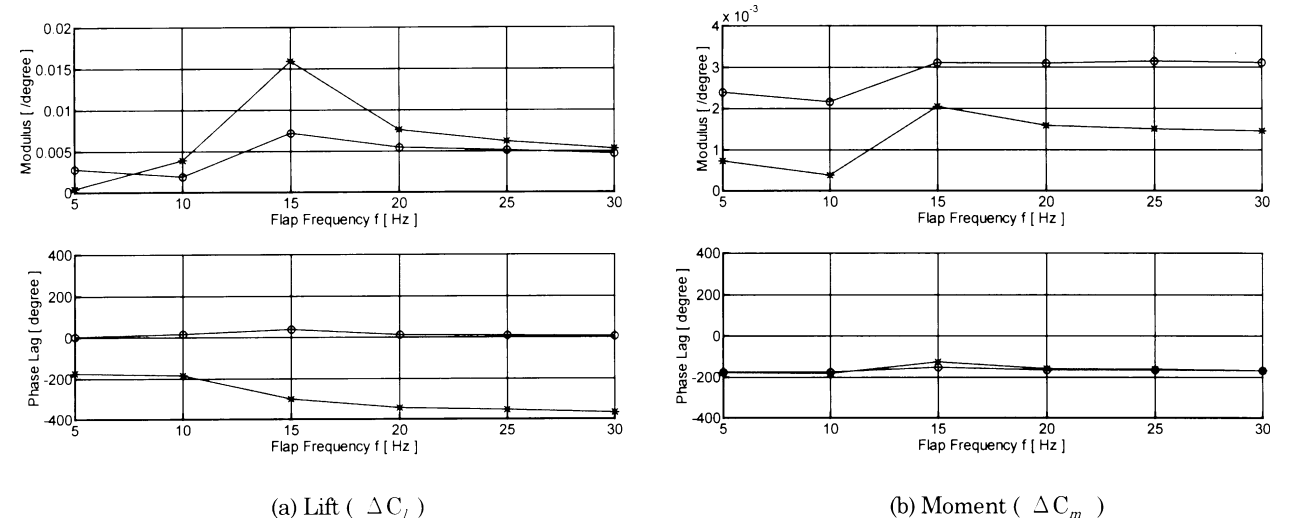
(f) $f = 30$ [Hz]

Figure 11. Pressure Distributions - Unsteady Component

(:Inboard Upper, :Inboard Lower, :Outboard Upper, :Outboard Lower)



(a) Lift (ΔC_l) (b) Moment (ΔC_m)
 Figure 12. Unsteady Component of Aerodynamic Force Coefficients
 (Upper : Inboard, Lower : Outboard)



(a) Lift (ΔC_l) (b) Moment (ΔC_m)
 Figure 13. Transfer Functions between Flap Motion and Aerodynamic Force Coefficients
 (◯ :Inboard, * :Outboard)

Figure 13 shows the transfer functions of C_l and C_m vs. the flap motions. The magnitude and the phase lag are presented. In the inboard region, the magnitudes of C_l and C_m do not show a steep peak at $f = 15$ Hz. The phase lag is almost 0 degree for C_l and 180 degrees for C_m . It is again noted that the influences of flap motions are strong in the inboard region. This statement is supported by the fact that the magnitudes of inboard C_m are greater than those of outboard.

In the outboard region, steeper peaks exist at $f = 15$ Hz in the magnitudes of C_l and C_m . These peaks are caused by almost the resonant vibration. The unsteady aerodynamic forces in the outboard are

strongly influenced by the model motions. The phase of C_l changes about 180 degrees around $f = 15$ Hz. This might show the change of model vibration mode as stated in the paragraphs 5.1 and 5.3.

6 . Concluding Remarks

Unsteady pressures and dynamic deformations were measured on a double-swept-back semi-span SST arrow wing model. The following conclusions were acquired.

- (1) Temperature drift in a wind tunnel generally influences pressure transducers and results in a static bias in the transducer signal. In this experi-

ment, the bias was removed by measuring the steady and unsteady pressure components separately. This also led to an improvement in the S/N ratio of unsteady pressure measurements.

(2) The wing 1st resonant frequency is about 13.5 Hz with $M = 0.851$ and $P_o = 80.0$ kPa. The effects of the pitching modes are greater at $f < 13.5$ Hz than $f > 13.5$ Hz. This change of wing vibrating mode could be found in the unsteady pressure data.

(3) Unsteady components of aerodynamic coefficients, that is, lift and moment around 25% chord, were calculated by integrating the unsteady pressure distributions at two semi-span positions. It is considered that the unsteady aerodynamic coefficients are strongly affected by the flap motion in the inboard region, while they are greatly influenced by the wing vibration mode in the outboard region.

7 . Acknowledgement

The authors would like to thank the staff of TWT including Mr. K. Suzuki of NAL and Mr. Y. Ando of JAST (Foundation for Promotion of Japanese Aerospace Technology) for their cooperation. We would also like to extend our thanks to Mr. H. Miwa of NAL and P. Granacy, who had been in NAL as an STA Fellow, for their useful suggestions during this research.

References

- (1) Boeing Commercial Airplanes: *High-Speed Civil Transport Study*, NASA CR 4233, 1989.
- (2) Takasu T. et al.: *Preliminary Sizing of a Supersonic Commercial Transport Between Mach 2.0 and 2.4*, SAE 965589, 1996.
- (3) Horsten J. et al.: *Unsteady Transonic Pressure Measurements on a Semi-span Wind-tunnel Model of a Transport-type Supercritical Wing (LANN Model)*, NLR TR 82069 U PartI, PartII, 1982.
- (4) *Compendium of Unsteady Aerodynamic Measurements*, AGARD-R-702, 1982.
- (5) Tijdeman H.: *Investigations of the Transonic Flow Around Oscillating Airfoils*, NLR TR 77090 U, 1977.
- (6) Abel I.: *Research and Applications in Aeroelasticity and Structural Dynamics at the NASA Langley Research Center*, Proceedings of CEAS International Forum on Aeroelasticity and Structural Dynamics Vol.I (1997), pp.51-68.
- (7) Tamayama, M. et al.: *Unsteady Aerodynamics Measurements on an Elastic Wing Model of SST*, AIAA 97-0836, 1997.
- (8) Honlinger, H. et al.: *Measurement of Wind Tunnel Model Deformation Under Airload*, Proceedings of CEAS International Forum on Aeroelasticity and Structural Dynamics (1989), pp.205-211.
- (9) Hashidate, M. et al.: *Development of Dynamic Deformation Measurement System*, Proceedings of 57th Meeting on Wind Tunnel Research, 1996 (in Japanese).
- (10) Tamayama M. et al.: *Measurements of Unsteady Pressure Distributions and Dynamic Deformations on an SST Elastic Wing Model*, Proceedings of CEAS International Forum on Aeroelasticity and Structural Dynamics Vol.III (1997), pp.231-238.
- (11) Suzuki, K. et al.: *Refurbishment of the NAL 2m × 2m Transonic wind tunnel test section*, NAL TM-674, 1995 (in Japanese).
- (12) Hashidate, M. et al.: *Wind Tunnel Tests of Arrow-Wing Flutter Model (No.1)*, Proceedings of 33rd Aircraft Symposium (1995), pp.329-332 (in Japanese).
- (13) Miwa, H. et al.: *Unsteady Pressure Measurements on the Aeroelastic SST Model - Measurements of Wide-band Spectrum and Propagation Velocity -*, Proceedings of 34th Aircraft Symposium (1996), pp.525-528 (in Japanese).